SURFACE ELECTRICAL CONDUCTION CORRELATED WITH SURFACE STRUCTURES AND ATOM DYNAMICS

SHUJI HASEGAWA,* CHUN-SHENG JIANG,[†]
YUJI NAKAJIMA[‡] and TADAAKI NAGAO
Department of Physics, School of Science, University of Tokyo,
7-3-1 Hongo, Bunkyo-ku, Tokyo 113-0033, Japan

XIAO TONG[§]
Core Research for Evolutional Science and Technology (CREST),
Japan Science and Technology Corporation (JST), Japan

By utilizing a variety of surface superstructures formed on silicon surfaces, we have clarified close correlations between the atomic-scale structures and surface-electrical-conduction phenomena. In particular, we have succeeded for the first time in experimentally confirming the electrical conduction via surface-state bands that are inherent in the surface supertructures. Also, an important phenomenon has been found: atoms adsorbed on the surface donate carriers to the surface-state band, resulting in a remarkable enhancement of conductivity. The ultimate two-dimensional electron systems composed of surface-state bands, which are made close up in our study, are expected to provide a new stage in surface physics.

1. Introduction

Silicon surfaces are undoubtedly the most important subject in surface science. A huge amount of knowledge about them has now been accumulated. In addition to superstructures formed on their clean surfaces, more than 300 kinds of "adsorbate-induced surface superstructures" on silicon have been found.[1] Detailed investigations of the atomic and electronic structures of the respective surfaces have been intensively carried out all over the world. However, there are a very limited number of studies for answering simple questions: What special properties do we actually have from the surface superstructures? Are there any electric, magnetic or optical proper-

ties at surfaces which are never exhibited in bulk? Expectations for novel properties and the resulting electronics devices are driving forces for researches on semiconductor surfaces. However, since structural/chemical analyses and their controls are not easy to do at all (therefore they are interesting), the properties of surfaces are seldom investigated by correlating them with the atomic-scale structures.

By utilizing a variety of the surface superstructures on silion surfaces, we have studied how the rearrangements of atoms only in one or two atomic layers on the topmost surfaces actually affect the electronic transport properties.[2] Recalling the history of modern surface physics, the electrical-conduction phenomena near semiconductor surfaces have

been one of the most important subjects since the discovery of transistors in the 1950's.[3] However, this subject does not seem to be involved in the mainstream of modern surface science, where structural controls and analyses on atomic scales are the main concerns. Instead, eletronic transport properties near semiconductor surfaces have been the main themes in mesoscopic physics and device physics where the arrangements and bondings of individual atoms near surfaces are not of interest. This is because the atomic-scale structures are believed to play no role in the transport properties. However, returning to the root of semiconductor surface physics, we intend to correlate the properties with the surface atomic structures.

In fact, we have succeeded for the first time in experimentally confirming the electrical conduction through a surface-state band inherent in a surface superstructure.[4] This demonstrates a good example of close correlation of the electrical properties with atomic structures. This type of conduction should be distinguished from the conventional surface electrical conduction through the surface space-charge layer. This new type of conduction is due to an inherently two-dimensional (2D) electron system localized only on the topmost surface atomic layer, while the conventional 2D electron system is made up of bulk-state electrons confined in space-charge layers at surfaces or heterojunctions. Therefore, we can expect some novel properties from the 2D electron system in surface-state bands, correlating with surface-structural modifications. Furthermore, an interesting phenomenon has been found: individual atoms adsorbed on a surface, which form a "2D adatom gas" phase, donate carriers into a surface-state band, resulting in a remarkable enhancement of conductance.[5,6] Nucleation of the adatoms into microcrystals from the gas phase diminishes the carrier-doping effect. From these findings, it can be reversely said that the measurements of surface electrical conduction may become a useful method for monitoring the surface atom dynamics in real time which are not directly observed in any microscopies or diffraction methods. In this paper, we intend to systematically describe our studies of the surface electrical conduction, which decisively depends on the atomic-scale structures and their dynamical changes.

2. Si(111)-(7 × 7) Clean and Si(111)-($\sqrt{3} \times \sqrt{3}$)-Ag Surfaces

First, we introduce two types of silicon surfaces which are investigated by comparing them in this paper.

A clean Si(111) surface reconstructs into a 7×7 superstructure whose atomic arrangement is now solved as DAS (dimer–adatom–stacking fault) structure Fig. 1(a).[7] Although this arrangement remarkably reduces the number of dangling bonds compared to an ideally truncated (111) surface, there still remain some of them. The dangling-bond state on each "adatom" on the topmost layer has an unpaired electron, resulting in a half-filled, and therefore metallic, surface-state band. This band is actually detected by angle-resolved ultraviolet photoelectron spectroscopy (ARUPS), denoted as "S_1" in the 2D band-dispersion diagram of Fig. 1(b). This surface state is always detected at the Fermi level (E_F) at any emission angles, indicating the Fermi-level pinning due to its high density of states. And this band is flat, negligible band dispersion. This is because the overlap integral between the neighboring dangling-bond states is so small that the electrons in this state are almost localized on the respective "adatoms." Therefore, electrical conductivity through the dangling-bond-state band is not expected to be very high in spite of its metallic nature. There are some experimental results suggesting a low DC conductance through the dangling-bond state.[8] Furthermore, the E_F at the surface, which is pinned by the S_1 band, is always located around the middle of the band gap, irrespective of the doping type and concentration in the bulk crystal,[9] so that the surface space-charge layer is always a depletion layer under the 7×7 surface [Fig. 1(c)]. Therefore, the electrical conduction through the surface space-charge layer is low, again.

Let us consider another surface, Si(111)-($\sqrt{3} \times \sqrt{3}$)-Ag, which is formed by depositing Ag atoms of one monolayer (ML) at elevated substrate temperatures. This sample has also been a popular target in surface science; after a long controversy, its atomic arrangement is now solved as HCT (honeycomb-chained trimers) structure proposed by Takahashi *et al.* [Fig. 1(d)].[10,11] The adsorbed Ag atoms form covalent bonds with the substrate Si atoms, leaving no dangling bonds on the surface. Thus an
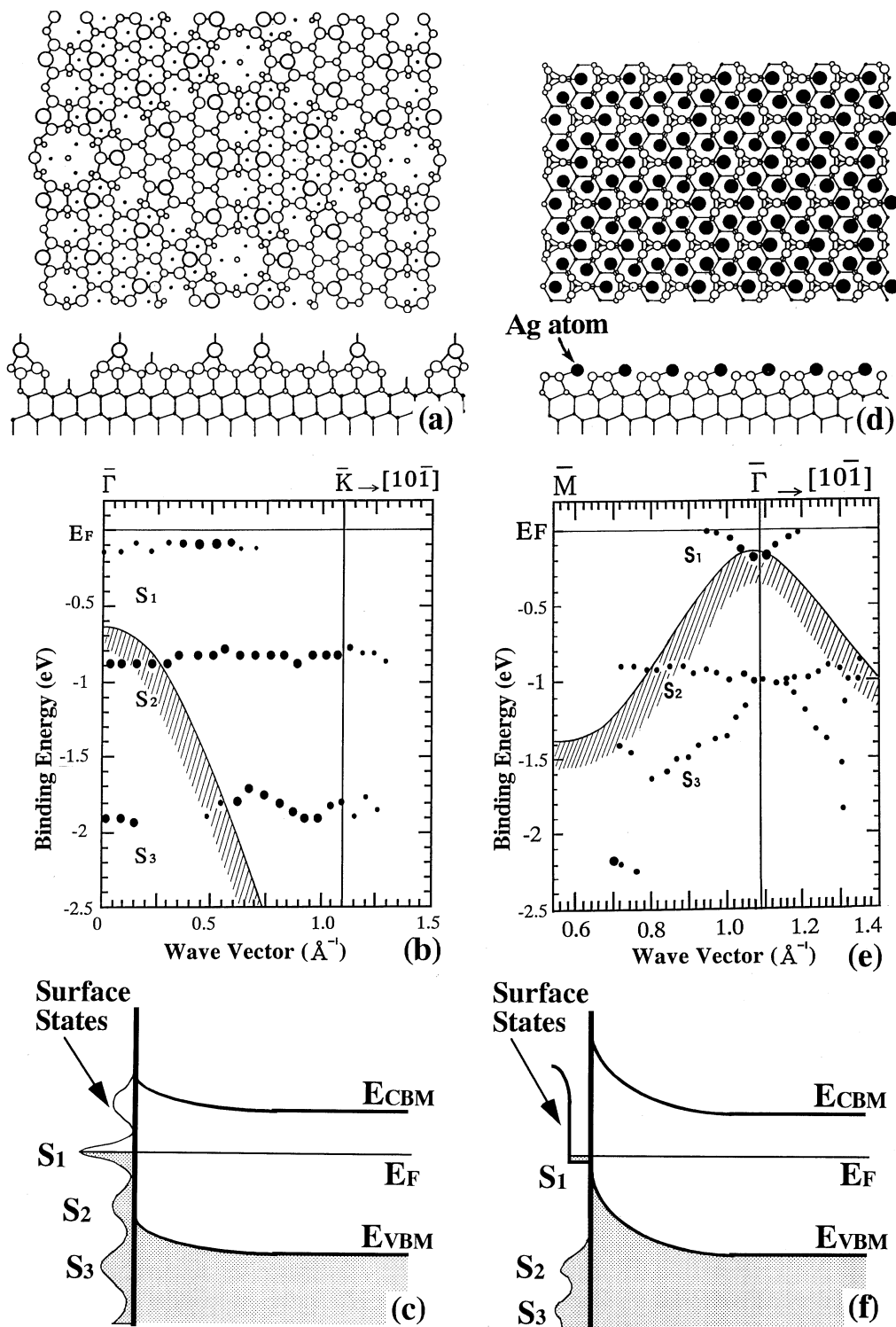
Fig. 1. (a)–(c) Si(111)-(7 × 7) clean surface and (d)–(f) Si(111)-($\sqrt{3} \times \sqrt{3}$)-Ag surface. (a), (d) Schematics of atomic arrangements (upper — plan view; lower — sectional view). (b), (e) Two-dimensional band-dispersion diagrams of surface states determined by angle-resolved ultraviolet photoelectron spectroscopy (ARUPS). Solid circles represent surface-state peaks in spectra, whose sizes roughly correspond to their intensities. $\overline{\Gamma}$ and $\overline{K}$ in (b) and $\overline{\Gamma}$ and $\overline{M}$ in (e) are symmetric points in the 1 × 1 and $\sqrt{3} \times \sqrt{3}$ surface Brillouin zones, respectively. The projected band structures of bulk are also included. (c), (f) Schematics of band diagrams showing surface states and surface space-charge layers.

energy gap opens up between the surface-state bands originating from antibonding and bonding states of Si–Ag bonds.[12] This is a semiconductor-like electronic structure. These states are also observed in ARUPS measurements, denoted as "S_1" and "S_2", respectively, in Fig. 1(e). We notice a peculiar feature in this band-dispersion diagram; a part of the antibonding-state band S_1 is observed below E_F, so that some electrons are trapped in this band. And this band is observed only in a narrow range of wave vectors around the $\overline{\Gamma}$ point and is highly upward-dispersive.[13] This means an extended electron wave function in this state, in contrast to the localized S_1-dangling-bond state at the 7×7 surface. Therefore, this situation is like a degenerate n-type semiconductor. This surface is thus expected to have a higher electrical conductance due to the excess electrons accumulated in the "surface-state conduction band S_1," in spite of its semiconducting nature. This situation of the surface electronic structure is almost irrespective of the bulk doping type and concentration. According to the first-principles calculations,[14] the local density of states of the S_1 surface-state band has a maximum at the centers of Ag trimers in the HCT framework, which is confirmed by STM observations.[15] Therefore, by recalling the high dispersion of the band, the electrons can be expected to travel via the Ag-trimer centers, resulting in a high conductance. It is also experimentally confirmed that the surface E_F is always located near the valence-band maximum,[16,13] so that the bands near the surface bend upwards, as shown in Fig. 1(f). The surface space-charge layer is thus a hole-accumulation layer to be highly conductive, again.

3. Surface Space-Charge Layer

As described above, the electrical-conduction phenomena near semiconductor surfaces are complicated. It is then very helpful to classify them into three types of conductions:[17]

(1) Conduction via a surface space-charge layer: excess charges trapped in the surface states cause the band bending below the surface, resulting in changes of carrier concentrations in the surface space-charge layer, whose width reaches several microns in a lightly doped semiconductor substrate. Although this is conduction through bulk states, the surface electronic states thus can decisively govern the electrical conductivity through the layer.

(2) Conduction via surface-state bands: two-dimensional bands are formed due to the surface superstructure. The electrons or holes in the bands should be mobile along the surface just like the carriers in the three-dimensional bulk bands, so that they contribute to electrical conduction. The conductivity of this type is directly dependent on the nature of the surface-state band (metallic or semiconducting) and also on the mobility of the carriers therein.

(3) Conduction via a grown atomic layer: if, for example, a metal atomic layer grows on a semiconductor surface at low temperatures, the grown layer dominates the conduction above a percolation-threshold coverage. Diffusivity of carrier scattering at surface/interface varies, depending on the morphology of the surface, leading to changes of carrier mobility. So the growth modes and kinetics, which are dependent on the surface structure, sensitively affect the conductivity.[18]

In this paper, we focus our attention only on the first two types, because we have mainly studied the very early stage of foreign atom adsorption on the surface, so that the conduction of type (3) is negligible.

Even though we measure the surface electrical conductance σ_s, we have to separately evaluate the contributions of types (1) and (2). This is because σ_s is a sum of the conductance through the surface space-charge layer σ_{sc} and that through the surface-state bands σ_{ss}; $\sigma_s = \sigma_{sc} + \sigma_{ss}$. Fortunately, it has already been established that σ_{sc} can be estimated if the surface and bulk E_F positions are known,[19] which is the basis of semiconductor devices. By solving the Poisson equation including the band bending determined by the difference of E_F positions between at surface and in deep bulk, the concentration of the excess carriers accumulated in the surface space-charge layer can be calculated. σ_{sc} will be obtained by multiplying the carrier mobilities with the calculated carrier concentrations; the mobilities can be assumed to be the same as those in the bulk unless the band bending is not so steep. The σ_{sc} obtained
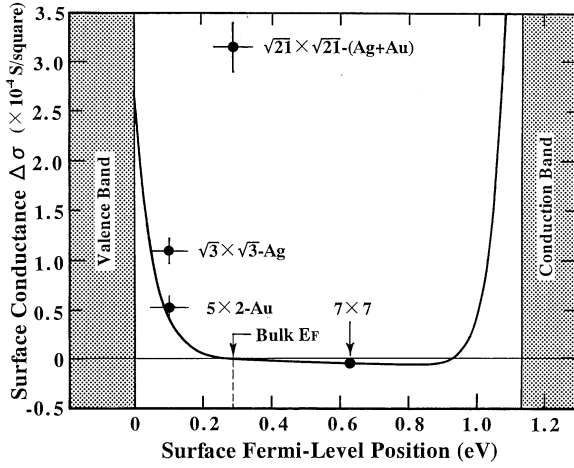
Fig. 2. A curve shows the conductance σ_{sc} through the surface space-charge layer, calculated as a function of the surface-E_F position for a p-type Si crystal of 20 Ω cm resistivity at room temperature. The difference of E_F positions between at surface and in deep bulk determines the band bending near the surface, under which condition we have solved the Poisson equation to obtain the excess carrier concentrations accumulated in the surface space-charge layer. By multiplying the mobilities (we have used the same values as in bulk) with the calculated carrier concentrations, we have finally obtained σ_{sc}. The σ_{sc} under the flat-band condition (under which the surface E_F coincides with the bulk E_F) is defined as zero, because no excess or depleted carriers are accumulated near the surface (the carrier concentrations are the same as in deep bulk). Moreover, by assuming that the extra conductivity due to the surface-state bands σ_{ss} is zero on the 7×7 clean surface, its data point is located on the calculated curve. The measured values of σ_s for the metal-covered surfaces $[(\sqrt{3} \times \sqrt{3})$-Ag, (5×2)-Au and $(\sqrt{21} \times \sqrt{21})$-(Ag + Au)], with reference to σ_s of the 7×7 clean surface, are plotted at the respective E_F positions. The E_F positions are determined by bulk-sensitive XPS. The data points of the $(\sqrt{3} \times \sqrt{3})$-Ag and (5×2)-Au surfaces are located near the calculated curve, while that of the $(\sqrt{21} \times \sqrt{21})$-(Ag + Au) surface is significantly above the curve.[4]

in this way is shown by a curve in Fig. 2 as a function of the surface E_F position.

When the surface E_F is located near the bulk valence-band maximum, E_{vbm}, the bands bend upwards so that the surface space-charge layer becomes a hole-accumulation layer where the excess holes are induced in the bulk valence band, resulting in enhancement of conductivity. When, reversely, the surface E_F is located near the bulk conduction-band minimum, E_{cbm}, the bands bend downwards so that the surface space-charge layer becomes an electron-

accumulation layer where the excess conduction electrons are induced in the bulk conduction band, resulting in enhancement of conductivity, again. If we include the carrier-scattering effect at the surface which results in reduction of their mobilities, the calculated curve of σ_{sc} will less steeply rise at both ends of the band gap. Between these extremes, i.e. when the surface E_F is located around the middle of the band gap, the surface space-charge layer is a depletion layer where the carriers are depleted from the region near the surface so that the conductivity is low.

The surface E_F positions of the respective surface superstructures can be determined with reference to that at the 7×7 clean surface.[9] By measuring the shifts of the Si 2p core-level position in X-ray photoelectron spectroscopy (XPS) with suitable photon energy of bulk-sensitive condition, the band bending can be directly determined, because any surface chemical shifts are negligibly detected under such a condition. The surface E_F positions at the 7×7 clean and the $(\sqrt{3} \times \sqrt{3})$-Ag surfaces are thus determined to be 0.63 eV[9] and 0.10 eV[16] above E_{vbm}, respectively.

By comparing the values of σ_{sc} at the respective E_F positions in Fig. 2, the conductance of the $(\sqrt{3} \times \sqrt{3})$-Ag surface is estimated to be higher than that of the 7×7 surface by about 50 μS/square. However, by measuring the conductance with a method described in the next section, σ_s of the $(\sqrt{3} \times \sqrt{3})$-Ag surface was higher by about 110 μS/square than that of the 7×7 surface, which was about double of the expected σ_{sc} difference. When this experimental value of σ_s is plotted at its surface E_F position in Fig. 2, the data point is located slightly above the calculated curve. This suggests some extra contribution of σ_{ss} in addition to σ_{sc}. But, by considering the experimental errors for determining the surface E_F position (about 0.1 eV) and $\sigma_s (\sim 10\%)$, and the uncertainty of the mobility values in calculating the curve in Fig. 2, it may be too early to conclude the contribution of σ_{ss}.[20] However, it was the Si(111)-$(\sqrt{21} \times \sqrt{21})$-(Ag + Au) surface described in Sec. 5 that unambiguously enabled us to confirm the contribution of the conductance through surface-state bands σ_{ss}.[4] As shown in Fig. 2, the data point of its σ_s deviates remarkably from the calculated curve of σ_{sc}, which means a significant contribution of σ_{ss} to σ_s. As discussed in Sec. 6, on the
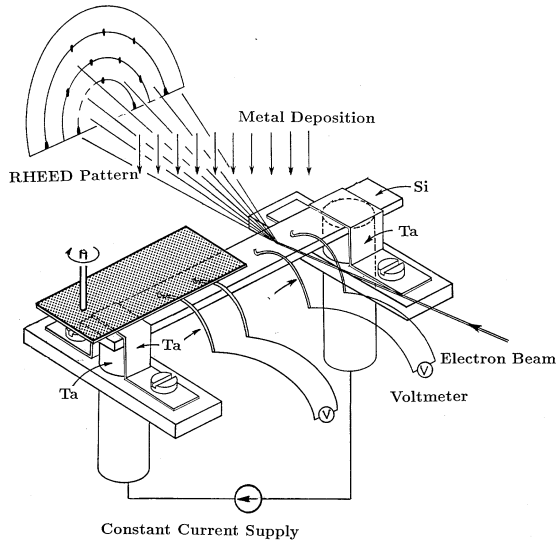
Fig. 3.   RHEED sample holder for the electrical-conductance measurements. Four Ta wires are pressed on the Si surface to pick up the voltage drops. By making the Si wafer flash heated up to 1200°C for cleaning with the wires in contact, the contact resistances between the Ta wire and the Si wafer tend to be stabilized. Since the electron beam for RHEED severely disturbs the electrical measurements, it is always turned off except for intermittent observations of the RHEED pattern.[20]

other hand, the electrical conduction through the S_1-surface-state band of the $(\sqrt{3} \times \sqrt{3})$-Ag surface has been confirmed through a conductance enhancement by carrier doping into the S_1 band by adsorbed atoms.[5,6]

4.   *In-Situ* Measurements of Surface Conductance in UHV

When the atoms rearrange only in one or two atomic layers on top of the surface, does the electrical resistance of a Si wafer with a macroscopic thickness (0.4 mm for our samples) actually change by detectable amounts? To answer this naive and interesting question, we made two surface areas of different surface superstructures on a single wafer to measure the respective resistance simultaneously.[20] As shown in Fig. 3, half of the Si wafer was masked from the evaporating Ag beam so that the 7×7 clean surface was kept on the half, while the other half of the surface changed into the $(\sqrt{3} \times \sqrt{3})$-Ag structure. The resistances of the two areas were simultaneously measured by making DC current
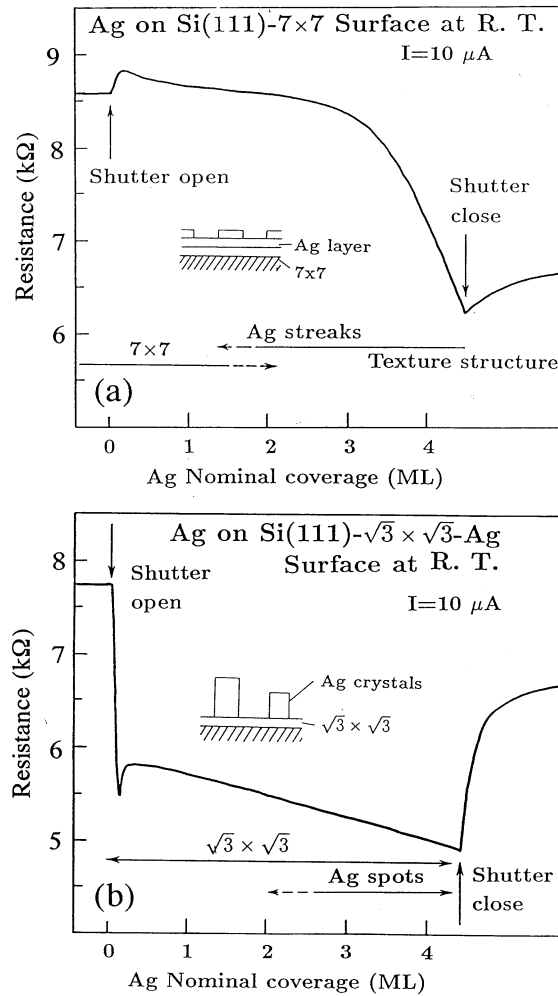
Fig. 4.   Resistance changes continuously measured during Ag depositions on (a) the Si(111)-(7×7) clean surface and (b) the Si(111)-($\sqrt{3} \times \sqrt{3}$)-Ag surface at room temperature. The Si crystal was $25 \times 4 \times 0.4$ mm^3 in size and n-type with 48–50 Ω cm resistivity. Changes in RHEED patterns observed in the separate runs of depositions under the same conditions are also indicated. Since the electrical conductivity in the deep bulk of Si wafer cannot be changed by this deposition, the resistance changes detected here are due to the conductivity changes only near the surface.[2]

$(1 \sim 200 \ \mu A)$ flow through the Ta clamps at both ends of the Si wafer, and by picking up the voltage drops between two pairs of Ta-wire contacts pressed on the respective areas. By this "six-probe method," we could measure the conductance difference originating only from the difference of surface superstructures, even if the conductance through the underlying bulk may change due to impurity redistributions
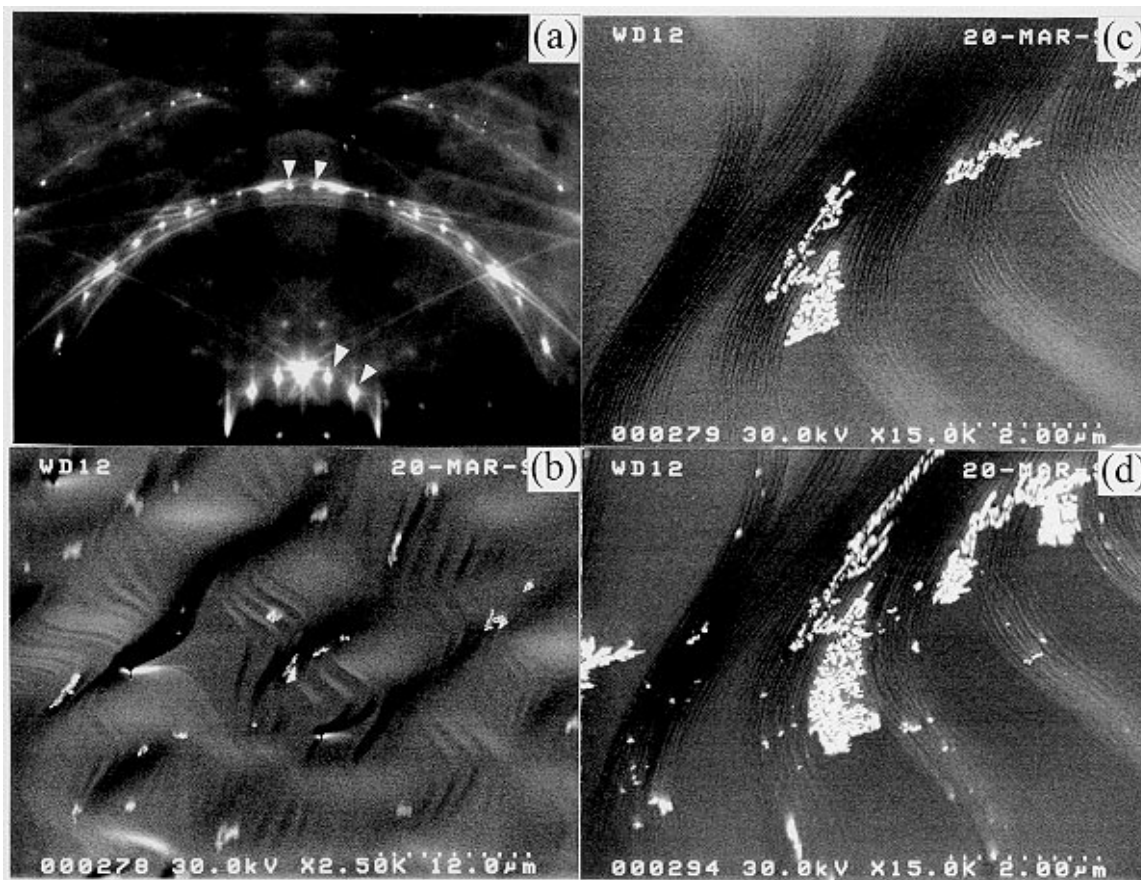
Fig. 5. (a) RHEED pattern taken after 4.5 ML Ag deposition on the Si(111)-($\sqrt{3} \times \sqrt{3}$)-Ag surface at room temperature. The intensities of the fractional-order spots indicated by arrowheads scarcely decrease by the deposition. This means that the deposited Ag atoms tend to nucleate into microcrystals, resulting in the surface being scarcely covered. In fact, transmission-type diffraction spots from 3D Ag microcrystals are seen in the pattern. (b) UHV-grazing-incidence scanning electron micrograph taken after deposition of about 0.2 ML Ag on the Si(111)-($\sqrt{3} \times \sqrt{3}$)-Ag surface at room temperature. (c) Its magnified image showing surface steps and "colonies" of 3D Ag microcrystals. (d) After additional deposition of about 0.2 ML Ag on the surface (c), the existing microcrystals do not grow; but, rather, additional microcrystals are newly formed. This is a heterogeneous nucleation process.[5]

in bulk raised by high-temperature flashings in UHV. The difference in σ_s between the ($\sqrt{3} \times \sqrt{3}$)-Ag and the 7×7 clean surfaces thus measured is plotted in Fig. 2.

During metal depositions, furthermore, *in-situ* and real-time measurements of resistance changes are possible by the conventional four-probe method with combining RHEED (reflection high-energy electron diffraction) observations. These methods enable one to correlate the resistance changes with dynamical structural changes such as growth styles of atomic layers, structural phase transitions, and so on.

Figure 4 shows the resistance changes during Ag deposition on a room-temperature substrate of (a) a Si(111)-(7×7) clean surface and (b) a Si(111)-($\sqrt{3} \times \sqrt{3}$)-Ag surface, respectively.[2] In (a), the resistance scarcely changes until about 3 ML (monolayer) coverage of Ag where the 7×7 superspots in the RHEED pattern almost disappear. Although the surface E_F shifts by about 0.25 eV towards the valence-band maximum during this period of deposition,[21,22] this amount of E_F shift is not enough to convert the surface space-charge layer into a hole-accumulation layer from the initial depletion layer. As a result, the conductance remains low. Moreover,

although the dangling-bond state on the clean 7×7 surface vanishes by Ag-atom adsorption, this change of the surface electronic state will not contribute to the conductance changes because the conductance through the dangling-bond state is inherently low, as mentioned in Sec. 2.[8] When Ag coverage exceeds 3 ML in Fig. 4(a), the resistance begins to decrease steeply, accompanying a change in the RHEED pattern showing a texture structure.[23] These indicate that Ag grows in a form of flat microcrystals, and that conductive percolation paths among them are formed by connecting each other.

In contrast to (a), a quite different phenomenon is observed on the $(\sqrt{3} \times \sqrt{3})$-Ag substrate in Fig. 4(b). The resistance suddenly drops just after the Ag deposition is started, and after passing through a small overshoot in the drop around Ag coverage as small as about 0.03 ML, the steep drop stops, followed by a gradual decrease with Ag coverage. During this process, the RHEED pattern shows a formation of 3D Ag microcrystals on the substrate, while the $\sqrt{3} \times \sqrt{3}$ superspots are scarcely weakened [Fig. 5(a)]. This indicates that the deposited Ag atoms can easily migrate to aggregate into the 3D Ag microcrystals, leaving the $(\sqrt{3} \times \sqrt{3})$-Ag surface scarcely covered. This nucleation process is confirmed also by UHV-SEM (scanning electron microscopy) observations, as shown in Figs. 5(b)–5(d). In spite of this surface being scarcely covered, the resistance of the whole surface is actually reduced. But, as shown in Fig. 4(b), when the Ag deposition is stopped by closing the evaporator shutter, the resistance steeply rises towards the initial value. One may guess at a glance that these resistance changes are caused by thermal radiation from the evaporator. But we have checked, using an empty evaporator heated up to the evaporating temperature, that it is not the case (see Fig. 3 in the first paper of Ref. 2). A "surface-state conduction band S_1" (mentioned in Sec. 2) plays an important role in these unusual behaviors of the electrical conductions on the $(\sqrt{3} \times \sqrt{3})$-Ag surface. Their mechanism will be solved in Sec. 6.

In this way, the electrical-conduction phenomena decisively depend on the surface superstructures of the substrate. In the case of depositions of Au,[2,22] In[2,24] and Pb,[25] also, similar phenomena of the resistance changes depending upon the surface struc-

tures have been found, though the details are of course different in the respective cases.

5. Electrical Conduction Through Surface-State Bands

Figure 6 shows the changes in the conductance and RHEED pattern during (a) Au adsorption at RT and (b) Ag adsorption at 200 K on the Si(111)-$(\sqrt{3} \times \sqrt{3})$-Ag surface. In both cases, $\sqrt{21} \times \sqrt{21}$ superstructures appear only in a coverage range of 0.08–0.3 ML [denoted as $(\sqrt{21} \times \sqrt{21})$-(Ag + Au) and $(\sqrt{21} \times \sqrt{21})$-Ag, respectively]. Figure 7 shows the RHEED pattern and STM image of the $(\sqrt{21} \times \sqrt{21})$-Ag surface, which indicate a well long-range-ordered structure in spite of adsorption at low substrate temperature. The conductances in both cases of Fig. 6 remarkably rise corresponding to the appearance of
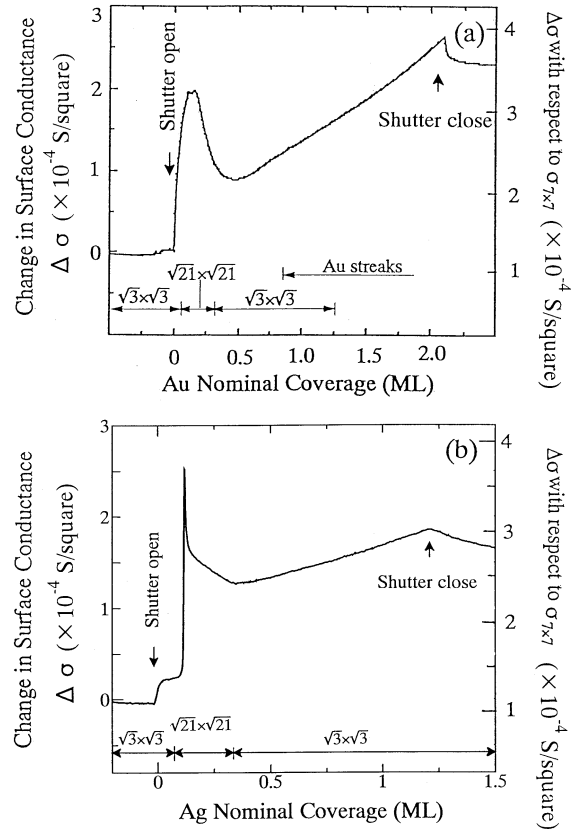
Fig. 6. Changes in the conductance and RHEED pattern of a Si wafer with the Si(111)-$(\sqrt{3} \times \sqrt{3})$-Ag surface continuously measured during (a) Au deposition at room temperature, and (b) Ag deposition at 200 K.[4] The Si crystal was p-type with 20 Ω cm resistivity.
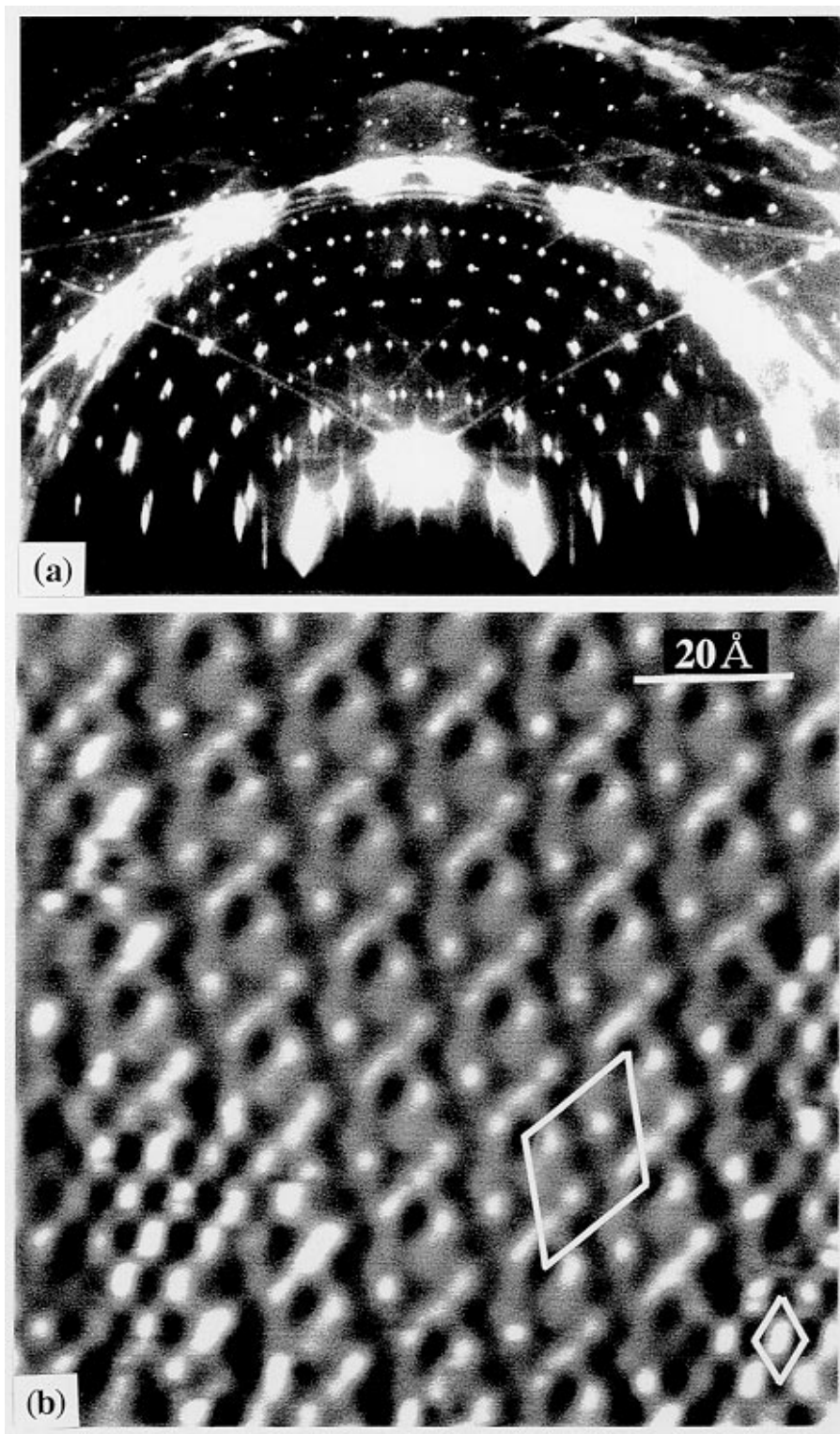
Fig. 7. Si(111)-($\sqrt{21} \times \sqrt{21}$)-Ag superstructure. (a) Its RHEED pattern observed *in situ* at 160 K during Ag deposition on the ($\sqrt{3} \times \sqrt{3}$)-Ag surface.[26] (b) Its STM image observed at 60 K, perpared at $\sim$ 150 K. The coverage of additional Ag was less than the saturation coverage ($\sim$ 0.15 ML), so that the underlying ($\sqrt{3} \times \sqrt{3}$)-Ag domains still remain (for example, at the lower left corner). Large and small lozenges indicate the unit cells of the $\sqrt{21} \times \sqrt{21}$ and $\sqrt{3} \times \sqrt{3}$ superstructures, respectively.

these $\sqrt{21} \times \sqrt{21}$ superstructures. As mentioned in Figs. 4(b) and 5, no changes in the surface superstructures were observed by Ag adsorption on the same $(\sqrt{3} \times \sqrt{3})$-Ag substrate at RT; the deposited Ag atoms just aggregate into 3D microcrystals. But at lower temperatures below 250 K, the surface migration of the deposited Ag atoms is suppressed to two-dimensionally cover the surface with the $\sqrt{21} \times \sqrt{21}$ superstructure.[26] In the case of Au adsorption, the superstructure can be formed even at RT because of their much smaller aggregation tendency. In both cases, however, the $\sqrt{21} \times \sqrt{21}$ superstructures complete around 0.15 ML deposition, and their atomic arrangements seem to be the same according to STM observations[27] and RHEED rocking-curve measurements.[28]

When the coverages exceed 0.3 ML, the $\sqrt{21} \times \sqrt{21}$ structures disappear to restore the $\sqrt{3} \times \sqrt{3}$ periodicity (Fig. 6). But their relative intensities among the $\sqrt{3} \times \sqrt{3}$ superspots in RHEED are different from those at the initial $(\sqrt{3} \times \sqrt{3})$-Ag surface. This means that atomic arrangements are different in spite of the same periodicity [denoted as $(\sqrt{3} \times \sqrt{3})$-(Ag + Au) in the case of Au adsorption]. Corresponding to these structural transformations from the $\sqrt{21} \times \sqrt{21}$ to the other $\sqrt{3} \times \sqrt{3}$ structures, the electrical conductances steeply decrease (Fig. 6). And then the conductances turn to gradual increases with coverage. We have also found that Cu deposition, as well as Au and Ag, induces very similar changes in structure and electrical conductance, formation of a similar $\sqrt{21} \times \sqrt{21}$ superstructure and a resulting remarkable increase of conductance.[27] However, because of limitation of space, we will focus our attention only on the $(\sqrt{21} \times \sqrt{21})$-(Ag + Au) surface induced by Au adsorption.

As seen in Fig. 6(a), the conductance makes a maximum around 0.15 ML Au coverage, of which value is plotted in Fig. 2 as the conductance σ_s of the $(\sqrt{21} \times \sqrt{21})$-(Ag + Au) surface. This data point remarkably deviates from the calculated curve. Figure 8 shows the shifts of surface E_F (band bending) during this Au deposition process, measured by XPS. At the initial $(\sqrt{3} \times \sqrt{3})$-Ag surface before Au deposition, the surface E_F is located around 0.1 eV above E_{vbm}, as mentioned in Sec. 2. But at the $(\sqrt{21} \times \sqrt{21})$-(Ag + Au) surface, it shifts to around 0.3 eV above E_{vbm}. This is almost the same position as in the deep bulk, so that the bands turn out
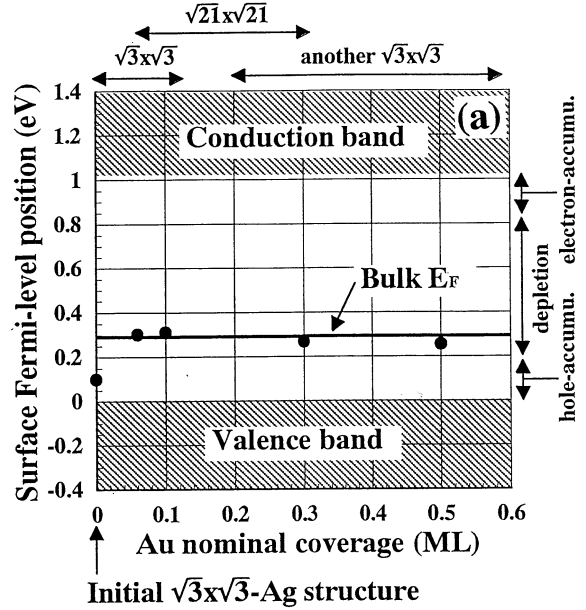
Fig. 8. Shifts of the surface Fermi-level position during Au adsorption onto the Si(111)-$(\sqrt{3} \times \sqrt{3})$-Ag surface at room temperature, measured through Si $2p$ core-level shifts in bulk-sensitive XPS.[4] The Si crystal was p-type with 20 Ω cm resistivity.

to be flat. This means that the excess holes accumulated in the surface space-charge layer under the initial $(\sqrt{3} \times \sqrt{3})$-Ag surface are depleted by Au adsorption. Therefore, as estimated from the curve in Fig. 2, the conductance via the surface space-charge layer σ_{sc} should be decreased by this E_F shift. On the contrary, the measured surface conductance σ_s significantly increases, coincidently with the formation of the $(\sqrt{21} \times \sqrt{21})$-(Ag + Au) structure. And the Au coverage (about 0.15 ML) needed for this superstructure is too small to make percolation paths on 2D triangular lattices.[29] As a consequence, we have to conclude that the surface-state bands of this superstructure make the conductance very high.[4]

We next show the electronic structure near E_F of this surface superstructure, investigated by ARUPS. In Fig. 9, the spectra in a range of emission angles $\theta_e = 25°–35°$ exhibit peaks near E_F, indicated by small arrowheads, which is called the S_1' surface state. This state is very similar to the S_1-state band of the initial $(\sqrt{3} \times \sqrt{3})$-Ag surface [see Fig. 1(e)]. Another surface-state band inherent in the $(\sqrt{21} \times \sqrt{21})$-(Ag + Au) superstructure is shown by big arrowheads in the spectra of $\theta_e = 30°–40°$, called the S_1^*
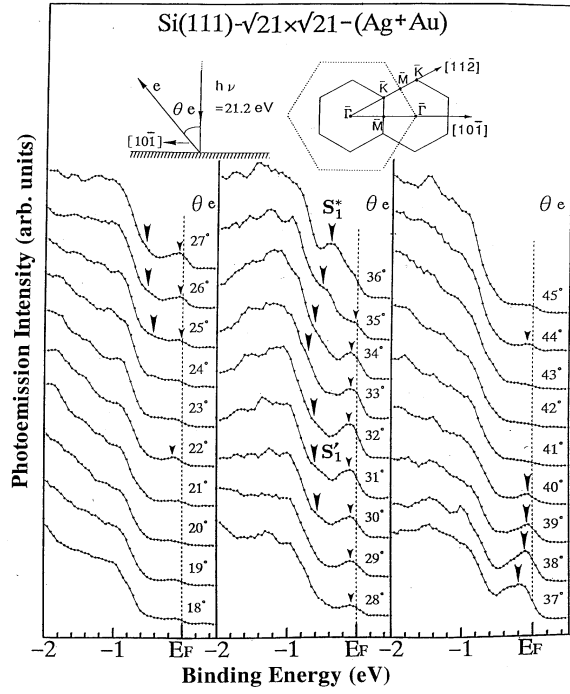
Fig. 9. Angle-resolved ultraviolet photoelectron spectra taken from the Si(111)-($\sqrt{21} \times \sqrt{21}$)-(Ag + Au) surface. The electron analyzer was scanned in the $[10\bar{1}]$ direction, and the electron emission angles θ_e were measured from the surface-normal direction. The range of θ_e shown here corresponds to around the $\overline{\Gamma}$ point in the second surface Brillouin zone. He I resonance light (21.2 eV) was used for excitation with irradiation in the surface normal. When the angle of incidence of the UV light was set off from the surface normal, the peak intensities of the surface states indicated by arrowheads were strongly suppressed, and almost disappeared at 45° incidence.[4,27]

Fig. 10. 2D band-dispersion diagram for the Si(111)-($\sqrt{21} \times \sqrt{21}$)-(Ag + Au) surface. $\overline{\Gamma}$ and $\overline{M}$ are symmetric points of the $\sqrt{3} \times \sqrt{3}$ surface Brillouin zone.[4,27] The projected bulk band structures are also included. The $\sqrt{21} \times \sqrt{21}$ symmetry in S_1^* and S_1' surface states is confirmed by scanning in other directions.[27]

state, which is not observed at the initial ($\sqrt{3} \times \sqrt{3}$)-Ag surface. A 2D band-dispersion diagram (Fig. 10) is constructed from these spectra. The S_1^* and S_1' bands are observed around the $\overline{\Gamma}$ point as the initial S_1 band in Fig. 1(e), and all of them are highly upward-dispersive, crossing E_F. The bottom of the S_1^* band is located as deep as 0.6 eV below E_F, which partially overlaps the projected bulk bands. The Fermi wave number k_F is given at a point where the band crosses E_F. The k_F of the S_1^* band is then approximately 0.2 Å^{-1}, while that of the S_1 band of the initial ($\sqrt{3} \times \sqrt{3}$)-Ag surface is about 0.1 Å^{-1}. That is to say, the radius of the Fermi disk (not a Fermi sphere because of two-dimensionality) of the surface-state band approximately doubles, so that the number of electrons contributing to

conduction is also roughly doubled. This increment of electrons trapped in the surface state is provided by adsorbed Au atoms, not from the bulk, because the surface space-charge layer is a depletion layer under the ($\sqrt{21} \times \sqrt{21}$)-(Ag + Au) structure. A semi-quantitative estimation shows that each Au adatom donates approximately 0.5 electrons to the surface-state band.[27] The adsorbed Au atoms act as donors to provide the conduction electrons to the surface-state band, and also to the surface space-charge layer to diminish the excess holes accumulated therein.

In this way, we have clarified that a high electrical conductance of the ($\sqrt{21} \times \sqrt{21}$)-(Ag + Au) surface is due to the S_1^*-surface-state band.[4] This is the first time anyone has experimentally confirmed the electrical conduction through a surface-state band by identifying it. Moreover, we can estimate

the carrier mobility μ in the surface-state band from the equation $\Delta\sigma_s = e \cdot \mu \cdot \Delta n$, where $\Delta\sigma_s$ is a difference of σ_s and Δn a difference of electron density in the surface states between the $(\sqrt{21} \times \sqrt{21})$-(Ag + Au) and $(\sqrt{3} \times \sqrt{3})$-Ag surfaces, estimated from Figs. 2 and 10. Since $\Delta\sigma_s \approx 2 \times 10^{-4}$ S/square and $\Delta n \approx 7 \times 10^{13}$ cm^{-2}, we find that $\mu \approx 20$ cm^2/V s at RT, which is much smaller than the bulk value $\mu_{bulk} \approx 1500$ cm^2/V s. This may be due to carrier scatterings by surface irregularities and phonons; scattering by phonons, especially, will much more severely affect the mobilities than in bulk, because of the monolayer thickness of our 2D electron system. But in order to fully understand the transport property in the surface-state bands, we have to directly measure the mobilities by Hall-effect or field-effect measurements to confirm this estimation.

By the way, what is the origin of the S_1^*-state band? How does it correlate with the atomic arrangement? As the structure itself of $(\sqrt{21} \times \sqrt{21})$-(Ag + Au) is not yet solved, it is impossible to answer this question at the present. Since, however, this superstructure is expected to consist of periodically arranged Au adatoms without breaking the underlying $(\sqrt{3} \times \sqrt{3})$-Ag framework,[30,31] we can make a guess of the answer. It is expected that the S_1^* and S_1' bands are originally the S_1 state of the $(\sqrt{3} \times \sqrt{3})$-Ag surface, which is partially modulated by electron transfer from Au adatoms. Recalling that the local density of states of the S_1 state has maxima at the centers of Ag trimers of HCT structure,[14] we guess that some of the Ag trimers are strongly modulated by Au adsorption to become the S_1^* state, while the remaining Ag trimers are not so influenced by Au adsorption to become the S_1' state, which is very similar to the initial S_1 state. The S_1'-state band can be said to be a remnant of the initial S_1 band, which is plausible if we consider the Au coverage to be as small as 0.15 ML. But, of course, we have to wait for theoretical calculations for the electronic structure based on a correct model of atomic arrangement to answer the above question.

6.   Dynamics of Adatoms and Surface Electrical Conduction

Now we try to clarify the strange change of resistance observed for the $(\sqrt{3} \times \sqrt{3})$-Ag surface in Fig. 4(b). How do we understand a remarkable resistance drop
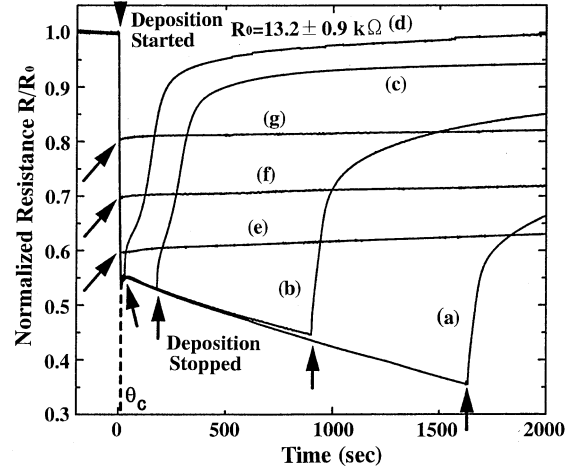
Fig. 11.   Resistance changes of a Si wafer with Si(111)-$(\sqrt{3} \times \sqrt{3})$-Ag surface at room temperature during and after additional Ag depositions (rate = 0.16 ML/min). The Si crystal was n-type with 100 Ω cm resistivity and $30 \times 4 \times 0.5$ mm^3 in size. The depositions were stopped at Ag coverages of (a) 4.5 ML, (b) 2.1 ML, (c) 0.52 ML, (d) 0.081 ML, (e) 0.025 ML, (f) 0.015 ML and (g) 0.0079 ML, respectively.[5]

by as large as more than 20%, induced by Ag adsorption of a coverage as small as 0.03 ML onto a Si wafer as thick as 0.4 mm? When, moreover, the Ag deposition is stopped at 4.3 ML Ag coverage by closing an evaporator shutter in Fig. 4(b), the resistance swiftly rises towards the initial value. In Figs. 11(a)–11(d), we made similar measurements, but the depositions were stopped at coverages of 4.5, 2.1, 0.52 and 0.081 ML, respectively. The resistances similarly rose towards the initial values, again, after the depositions. However, in Figs. 11(e)–11(g), where the depositions were stopped at 0.025, 0.015 and 0.0079 ML coverages, respectively (which are in the course of the initial steep drop of resistance), the resistances were, surprisingly, kept constant after stopping the depositions! The resistance changes after the depositions are thus revealed to be completely different, depending on whether the Ag coverage is more than a critical coverage θ_c (~ 0.03 ML) or less than θ_c.[5] θ_c corresponds to Ag coverage at a small overshoot at the initial resistance drop in Figs. 4(b) and 11.

Shown in Fig. 12(a) is a resistance change when the Ag is deposited with some interruptions.[5] In this case, again, the resistance remains constant during the interruption intervals A, B and C, where the Ag
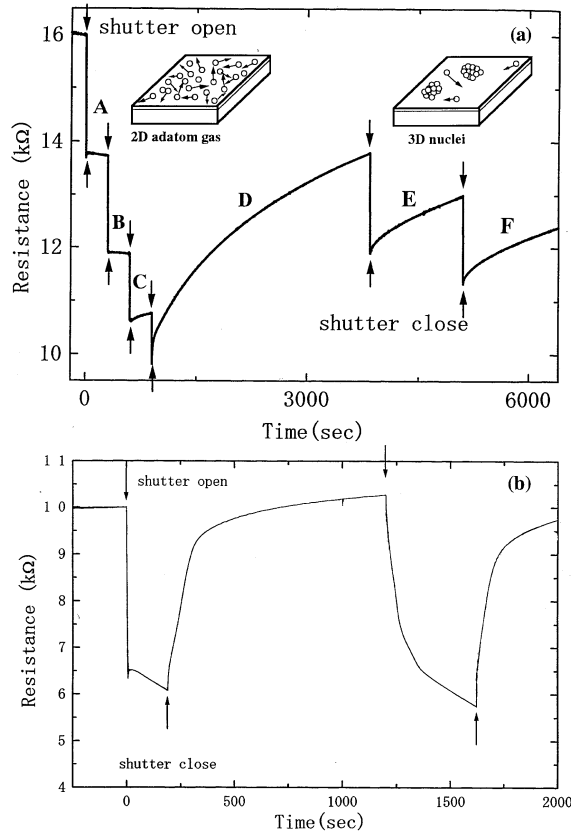
Fig. 12. (a) A resistance change of a Si wafer during intermittant Ag depositions (rate = 0.24 ML/min) on the Si(111)-($\sqrt{3} \times \sqrt{3}$)-Ag surface at room temperature. The Si wafer was n-type with 100 Ω cm resistivity. Downward arrows indicate the starting points of depositions, and upward arrows their end points. Ag atoms of the amount of 0.008 ML are deposited during each deposition period of 2 s. A–F indicate the interruption intervals.[5] (b) A resistance change during two successive Ag depositions on the same surface. Ag of 0.5 ML is deposited at the first deposition, and after about a 17 min interval, 2.2 ML is deposited at the second period.[5]

coverage is below θ_c. But, once the coverage exceed θ_c, the resistance rises towards the initial value during the interruption intervals D, E and F.

The RHEED and SEM observations shown in Fig. 5 indicate that Ag atoms deposited on the room-temperature ($\sqrt{3} \times \sqrt{3}$)-Ag surface nucleate into 3D microcrystals. By considering this structural change, the above-mentioned resistance changes are interpreted as follows. In general, to make the nucleation set on, the density of the deposited atoms should exceed a critical density of adatoms θ_c (critical supersaturation). In other words, when the coverage

is less than θ_c, the nucleation does not proceed, and the deposited atoms remain isolated, forming a supersaturated metastable "2D adatom gas (2DAG)" phase. Then, it is naturally understood that Ag atoms in the 2DAG phase before being incorporated into 3D microcrystal nuclei can make the resistance low, and that the resistance drops observed in Figs. 4(b), 11 and 12(a) correspond to the increments of the atom density in the 2DAG phase. Up to θ_c, the density of 2DAG increases by deposition, resulting in the resistance drop. Even if the deposition is stopped at this stage, 2DAG remains metastable to keep the gas density constant, and therefore the resistance remains constant. But once the adatom density exceeds θ_c, the nucleation sets on with capture of the atoms in the 2DAG phase by stable nuclei. If the deposition is stopped at this stage, the density of 2DAG decreases by nucleation, and will reach a very low density equilibrated with the nuclei. This process makes a resistance rise towards the initial values. This change of adatom density in the gas phase is revealed by a Monte Carulo simulation.[32] We cannot directly observe the individual adatoms in the 2DAG phase by RHEED, SEM or STM, because they are highly mobile.[2] Only the stable nuclei (3D microcrystals) can be observed. As shown in the micrograph of Fig. 5, the 3D microrystals tend to gather together to make "colonies." The distances among the colonies are as large as the order of 1 μm. This indicates that Ag atoms in the 2DAG phase are so mobile that they can easily migrate across atomic steps on the surface to make their surface diffusion lengths very long.

We have found another phenomenon which supports the scenario that the 2DAG phase reduces the electrical resistance.[5] Figure 12(b) shows a resistance change during two successive Ag depositions on the ($\sqrt{3} \times \sqrt{3}$)-Ag at RT. Ag atoms of 0.5 ML are deposited at the first deposition, and after about a 17 min interruption, the second deposition of 2.2 ML coverage is started. The resistance changes observed during and after these two depositions look similar; the initial steep drop, the following gradual decrease and the steep rise after the depositions off. But, on closer observation, we notice a difference — the overshoot at the initial resistance drop appears around 0.03 ML coverage only in the first deposition, but not in the second deposition, where instead a gradual transition from the initial steep drop to the

following gradual decrease is observed. This can be interpreted to correspond to a kinetic overshoot for beginning the nucleation only in the first deposition. At the first deposition on a "fresh" $(\sqrt{3} \times \sqrt{3})$-Ag surface ("fresh" means that there are no stable nuclei in a range of diffusion lengths of deposited Ag atoms which may act as sinks for the gas-phase Ag adatoms), the density of Ag adatoms kinetically exceeds the critical supersaturation density before their nucleation starts. This temporary excess density of adatoms is observed as an overshoot of the resistance drop in the first deposition in Fig. 12(b) [and also in Figs. 4(b) and 11]. In the second deposition, on the other hand, there already exist stable nuclei with separations of diffusion lengths of Ag adatoms on the surface, which were formed in the first deposition, so that the deposited atoms are swiftly captured by the nuclei. This is the reason why the adatom density does not exceed so much beyond the critical supersaturation density that no overshoot appears in the resistance drop during the second deposition in Fig. 12(b). From these observations and considerations, in other words, to measure the resistance changes in real time can turn into a method for monitoring atomistic dynamics which cannot be observed by microscopies and diffractions.

Then we have to face the next questions. Why do only the Ag atoms in 2DAG phase reduce the resistance? Why do they lose such a function once nucleated into 3D microcrystals? To answer these questions, we have done photoemission spectroscopies at RT for three surfaces: (a) the "fresh" $(\sqrt{3} \times \sqrt{3})$-Ag surface (without additional Ag deposition), (b) the same surface with 2DAG on it (additional Ag of 0.022 ML), and (c) the same surface with 3D microcrystals on it (additional Ag of 0.088 ML). Since, as shown in Figs. 11(e)–11(g), the 2DAG can remain on the surface for at least one hour to keep the resistance low, we can measure photoemission spectroscopies during it. At first, in the same way as described in Sec. 3, we did XPS to determine the band bendings at the respective surfaces. The peak of Si 2p core level was found to shift towards higher binding energy by 0.18 eV from at the surface (a) to (b), while the peaks at the surface (c) shifted back to the initial position at the surface (a).[6] As mentioned in Sec. 2, the bands below the "fresh" $(\sqrt{3} \times \sqrt{3})$-Ag surface bend upwards so that the surface space-charge layer is a hole-accumulation layer. But, the

above results of XPS tell us that 2DAG makes the bands bend towards the flat-band situation, resulting in sweeping out the excess holes accumulated in the surface space-charge layer. Therefore, 2DAG reduces the conductance σ_{sc} through the surface space-charge layer. This is completely opposite to the resistance drops observed in Figs. 4(b) and 11. As a consequence, we have to include σ_{ss}, the surface-state conduction, again. This is because the additional Ag coverage of 0.03 ML is of course too small to form percolation paths.

Next, we measured ARUPS from the respective surfaces. Figures 13(a) and 13(b) show the spectra taken from the surfaces (a) and (b), respectively, scanned in the $[10\bar{1}]$ direction around the $\bar{\Gamma}$ point in the second surface Brillouin zone.[6] Three peaks, indicated by arrowheads, correspond respectively to the surface states S_1, S_2 and S_3, which exhibit characteristic dispersions. These features in spectra scarcely change from at the surface (a) to (b), but the binding energies of the respective states shift. The changes are more clearly observed in the 2D band-dispersion diagram in Fig. 14.[6] The three surface states at the "fresh" $(\sqrt{3} \times \sqrt{3})$-Ag surface (a) of course disperse in the same way as in Fig. 1(e). These states at the surface (b) on which 2DAG rides shift downward by 0.15 eV compared to at the surface (a), though no significant changes in dispersion. Furthermore, when
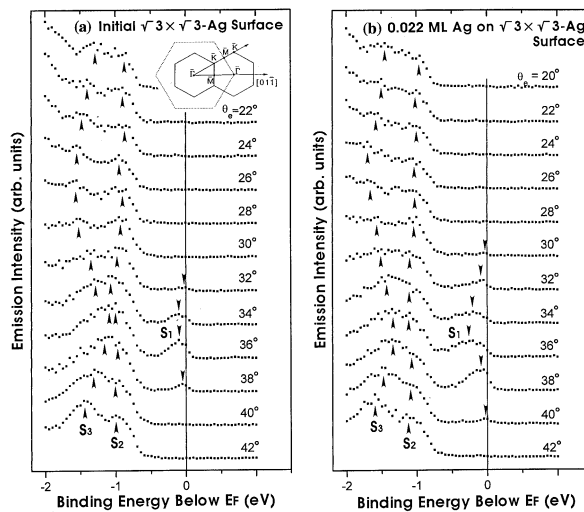
Fig. 13.   ARUPS measurements in the same way as in Fig. 9 for (a) "fresh" $(\sqrt{3} \times \sqrt{3})$-Ag surface and (b) the same surface with 2DAG of 0.022 ML Ag on it, respectively.[6]
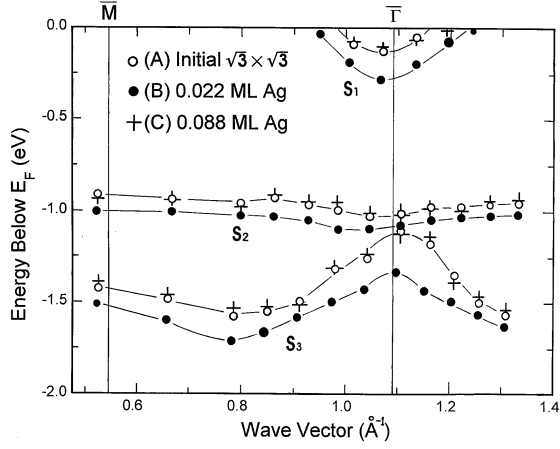
Fig. 14. 2D band-dispersion diagram obtained from the spectra in Fig. 13 for three surfaces: (A) "fresh" $(\sqrt{3} \times \sqrt{3})$-Ag surface (open circles), (B) 0.022 ML Ag 2DAG on it (closed circles), and (C) 0.088 ML Ag 3D microcrystals on it (crosses), respectively. Three surface states, S_1, S_2 and S_3, are plotted. $\overline{\Gamma}$ and $\overline{M}$ indicate the symmetric point in the second $\sqrt{3} \times \sqrt{3}$ surface Brillouin zone.[6]

2DAG nucleates into 3D microcrystals on the surface (c), these states return to almost the same position as at the surface (a).

Especially, focusing on the behavior of S_1-state band crossing E_F, the occupation in this band increases from the surface (a) to (b), and accordingly the intensity of its peak in spectra of Fig. 13 increases. That is to say, more electrons are trapped in the surface-state conduction band S_1, leading to an increase of conductivity. More strictly speaking, as discussed in Sec. 5, the Fermi wave number k_F is approximately 0.1 Å^{-1} at the surface (a), while it increases to be $k_F \approx 0.15$ Å^{-1} at the surface (b), so that the Fermi disk becomes larger to increase the number of electrons contributing to conduction.[6] Therefore, it can be said that Ag adatoms in the 2DAG phase act as donors to provide conduction electrons to the surface-state conduction band S_1. At the same time, the adatoms donate electrons also to the surface space-charge layer to diminish the excess holes therein.

By estimating the sum of electrons transferred into the S_1 band and into the surface space-charge layer, and by comparing it with the density of the deposited Ag adatoms, it is found that each Ag adatom donates approximately one electron, 97% of which goes into the S_1 band and 3% into the surface space-charge layer. Moreover, by comparing the increments of conductance $\Delta\sigma_s$ and electron density Δn in the S_1 band, the mobility μ of the conduction electrons in the S_1 band is estimated by $\mu = \Delta\sigma_s / e \cdot \Delta n$ to be around 10 cm^2/V$_s$.[6] This value of mobility is similar to on the $(\sqrt{21} \times \sqrt{21})$-(Ag + Au) surface discussed in Sec. 5.

This donor-type action of Ag adatom gas is similar to Au adatoms in the $(\sqrt{21} \times \sqrt{21})$-(Ag + Au) superstructure described in Sec. 5. However, in the case of adatom gas, new surface-state bands such as S_1^* and S_1' bands at the $(\sqrt{21} \times \sqrt{21})$-(Ag + Au) surface are not formed; but, rather, the original S_1 band just shifts. Since Ag adatoms act as donors, they are positively charged. This sign of charge is consistent with observations of electromigration.[33] As the results of XPS and ARUPS at the surface (c) return to almost the same ones at the surface (a), it can be said that the electron transfer from the adsorbates to the substrate or the donor action of Ag atoms vanishes once they nucleate into 3D microcrystals. This makes the conductance return to the initial lower value.

7. Concluding Remarks: 2D Electron Systems Made up of Surface-State Bands

From a series of our studies discussed in this paper, the electrical-conduction phenomena via surface-state bands have been clarified only on a stage of the Si(111)-$(\sqrt{3} \times \sqrt{3})$-Ag surface. But we believe that this type of electrical conduction is a general phenomenon which should be observed on surfaces having a "surface-state conduction band" (which is not necessarily metallic). Our studies are just a starting point of systematic investigations of the electronic transport properties of such an ultimate 2D electron system made up of surface-state bands, where the correlation with the atomic arrangements on surfaces is essential. This point contrasts with mesoscopic physics. For example, carrier scatterings by a variety of atomistic irregularities on surface can be directly investigated. STM in fact has enabled one to image electron standing waves due to scattering of electrons in surface-state bands by atomic steps or defects on single-crystal Au and Cu surface.[34,35] As one can easily imagine from those STM pictures, the

mobilities of carriers in surface-state bands will be sensitively affected by atomic structures on surfaces. On the other hand, by utilizing the variety of surface superstructures which is not exhibited in bulk, we will be able to control the transport properties in novel ways. In the near future, the huge amount of knowledge of the atomic and electronic structures of silicon surfaces accumulated so far, will bring to fruition a new, rich field of research on surface electronic transport properties.

Acknowledgments

References

1. V. G. Lifshits, A. A. Saranin and A. V. Zotov, *Surface Phases on Silicon* (John Wiley and Sons, Chichester, 1994).

2. S. Hasegawa and S. Ino, *Phys. Rev. Lett.* **68**, 1192 (1992); *Surf. Sci.* **283**, 438 (1993); *Thin Solid Films* **228**, 113 (1993); *Int. J. Mod. Phys.* **B7**, 3817 (1993); in *Nanostructures and Quantum Effects*, eds. H. Sakaki and H. Noge (Springer, Berlin, 1994), p. 104.

3. M. Kikuchi, *Buturi* **51**, 21 (1996) (in Japanese).

4. C.-S. Jiang, X. Tong, S. Hasegawa and S. Ino, *Surf. Sci.* **376**, 69 (1997); S. Hasegawa, X. Tong, C.-S. Jiang, Y. Nakajima and T. Nagao, *Surf. Sci.* **B86**, 322 (1997).

5. Y. Nakajima, G. Uchida, T. Nagao and S. Hasegawa, *Phys. Rev.* **B54**, 14134 (1996).

6. Y. Nakajima, X. Tong, T. Nagao, S. Takeda and S. Hasegawa, *Phys. Rev.* **B56**, 6782 (1997).

7. K. Takayanagi, Y. Tanishiro, M. Takahashi and S. Takahashi, *J. Vac. Sci. Technol.* **A3**, 1502 (1985); *Surf. Sci.* **164**, 367 (1985).

8. Ph. Avouris, I.-W. Lyo and Y. Hasegawa, in *Chemical, Structural and Electronic Analysis of Hetro-geneous Surfaces on Nanometer Scale*, ed. R. Rosei (Kluwer, 1997), p. 1; V. A. Gasparov and K. R. Nikolaev, *Phys. Low-Dim. Struct.* **1/2**, 53 (1996).

9. F. J. Himpsel, G. Hollinger and R. A. Pollack, *Phys. Rev.* **B28**, 7014 (1983).

10. T. Takahashi and S. Nakatani, *Surf. Sci.* **282**, 17 (1993), and references therein.

11. M. Katayama, R. S. Williams, M. Kato, E. Nomura and M. Aono, *Phys. Rev. Lett.* **66**, 2762 (1991).

12. T. Yokotsuka, S. Kono, S. Suzuki and T. Sagawa, *Surf. Sci.* **127**, 35 (1983).

13. L. S. O. Johansson, E. Landemark, C. J. Karlsson and R. I. G. Uhrberg, *Phys. Rev. Lett.* **63**, 2092 (1989); *ibid.* **69**, 2451 (1992).

14. S. Watanabe, M. Aono and M. Tsukada, *Phys. Rev.* **B44**, 8330 (1991): Y. G. Ding, C. T. Chan and K. M. Ho, *Phys. Rev. Lett.* **67**, 1454 (1991); *ibid.* **69**, 2452 (1992).

15. K. J. Wan, X. F. Lin and J. Nogami, *Phys. Rev.* **B45**, 9509 (1992).

16. S. Kono, K. Higashiyama, T. Kinoshita, T. Miyahara, H. Kato, H. Ohsawa, Y. Enta, F. Maeda and Y. Yaegashi, *Phys. Rev. Lett.* **58**, 1555 (1987).

17. M. Henzler, in *Surface Physics of Materials I*, ed. J. M. Blakely (Academic, New York, 1975), p. 241.

18. For example, J. T. Coutts, *Electrical Conduction in Thin Metal Films* (Elsevier, Amsterdam, 1974); M. Jalochowski and E. Bauer, *Phys. Rev.* **B37**, 8622 (1988); *Phys. Rev.* **B38**, 5272 (1988); *Surf. Sci.* **213**, 556 (1989).

19. D. R. Frankl, *Electrical Properties of Semiconductor Surfaces* (Pergamon, 1967); S. M. Sze, *Physics of Semiconductor Devices* (John Wiley and Sons, New York, 1981).

20. C.-S.Jiang, S. Hasegawa and S. Ino, *Phys. Rev.* **B54**, 10389 (1996).

21.. J.-J. Yeh, J. Hwang, K. Bertness, D. J. Friedman, R. Cao and I. Lindau, *Phys. Rev. Lett.* **70**, 3768 (1993); A. Samsavar, T. Miller and T.-C. Chiang, *Phys. Rev.* **B42**, 9245 (1990).

22. S. Hasegawa, C.-S. Jiang, X. Tong and Y. Nakajima, *Advances in Colloid and Interface Science* **71—72**, 125 (1997).

23. Y. Goto and S. Ino, *Jpn. J. Appl. Phys* **17**, 2097 (1978); *Thin Solid Films* **109**, 255 (1983).

24. S. Takeda, T. Nagao, S. Ino and S. Hasegawa, submitted to *Surf. Sci.*

25. X. Tong, K. Horikoshi and S. Hasegawa, to be published in *Phys. Rev. B*.

26. X. Tong, S. Hasegawa and S. Ino, *Phys. Rev.* **B55**, 1310 (1997): Z. H. Zhang, S. Hasegawa and S. Ino, *Phys. Rev.* **B52**, 10760 (1995).

27. X. Tong, C.-S. Jiang, and S. Hasegawa, *Phys. Rev.* **B57**, 9015 (1998); X. Tong, thesis (University of Tokyo, 1997).

28. M. Lijadi, H. Iwashige and A. Ichimiya, *Surf. Sci.* **357—358**, 51 (1996).
29. R. Schad, S. Heun, T. Heidenblut and M. Henzler, *Phys. Rev.* **B45**, 11430 (1992).
30. J. Nogami, K. J. Wan and X. F. Lin, *Surf. Sci.* **306**, 81 (1994).
31. A. Ichimiya, H. Nomura, Y. Horio, T. Sato, T. Sueyoshi and M. Twatsuki, *Surf. Rev. Lett.* **1**, 1 (1994).
32. A. Natori, M. Murayama and H. Yasunaga, *Surf. Sci.* **357/358**, 47 (1996).
33. H. Yasunaga and A. Natori, *Surf. Sci. Rep.* **15**, 205 (1992).
34. Y. Hasegawa and Ph. Avouris, *Phys. Rev. Lett.* **71**, 1071 (1993).
35. M. F. Crommie, C. P. Lutz and D. M. Eigler, *Nature* **363**, 524 (1993).